Protections 2016 Ft. Collins, Colorado, USA, 7-9 September 2016
2nd International Seminar on
Dam Protection Against Overtopping
ISBN: 978-1-1889143-27-9 DOI:

Insights from Laboratory Experiments on the Failure of Earthen Embankments at Bridge-Waterway Abutments

R. Ettema[1] and K.W. Ng[2]
[1]Dept. of Civil & Environmental Engineering
Colorado State University
Ft. Collins, CO 80523
USA
[2]Dept. of Civil & Architectural Engineering
University of Wyoming
Laramie, WY 82071
USA
E-mail: rettema@colostate.edu

ABSTRACT

Failure of compacted, earthfill embankments during breaching combines geotechnical and hydraulic processes that interact to erode the compacted earthfill. Our paper offers insights regarding these processes as observed during a series of laboratory flume experiments conducted to investigate the effect of soil strength on scour depth at abutments formed of erodible, compacted earthen approach embankment. The length scale of the model abutments was 1:30. We highlight the challenges in conducting laboratory experiments involving erodible model abutments. The challenges, or difficulties, include attaining scale-reduced shear strengths, controlling and verifying the soil compaction, and quantifying the in-situ shear strength of both non-cohesive and cohesive model soils. We addressed these difficulties through a sequence of soil tests designed to relate model soil strength to laboratory compaction, using hand-held devices to check soil strengths in the flume experiments. Our paper explains the successes and unresolved issues relating to the shear strength of model soils used in flume studies of embankment breaching. Additionally, our paper illustrates the importance of large-scale turbulence structures formed at the breach entrance in shaping the breach, and discusses the geotechnical manner whereby breaches widen.

Keywords: *earthen embankments, dams, levees, abutments, erosion*

1. INTRODUCTION

Although embankment breaching is a common cause of earthen embankment failure, further research is needed to determine how geotechnical and hydraulics processes combine during breach development. Earthen embankments used for approaches to bridge-waterway abutments, as well as embankments for dams and levees, are susceptible to breaching. Our paper offers insights from laboratory experiments on erosion of earthen embankments at bridge abutments. We suggest that the breaching of bridge embankments during abutment scour involves facets of the same combined hydraulics and geotechnical processes at play in embankment dam breaching once a breach forms. We offer the following insights from laboratory experiments on abutment scour (Ettema et al. 2016, Ettema et al. 2010 and Ng et al. 2015):

- Large-scale turbulence structures, and water waviness, at the entrance corners of a breach substantially augmenting the effects of flow acceleration through a developing breach.
- Rather than slip-surface failure occurring, as assumed in leading numerical models of breach development (e.g., Wu et al. 2013), geotechnical failure involves under-cutting and toppling of soil blocks.
- Techniques for preparing scale-reduced, model soils for use in laboratory experiments of breaching may influence experiment results

Studies of embankment breaching recognize the importance of embankment soil strength in determining the rate and extent of breach development, but most appear to treat soil strength indirectly (e.g., as summarized in Brunner 2014). Morris (2007), ASCE Task Committee on Dam/Levee Breaching (2011), Feliciano-Cestero et al. (2014), and others, discuss how soil strength influences earthen dam and levee failure due to overtopping during floods. We concur with their statement that the scale effects associated with modelling cohesive soils during flume experiments are not sufficiently well established.

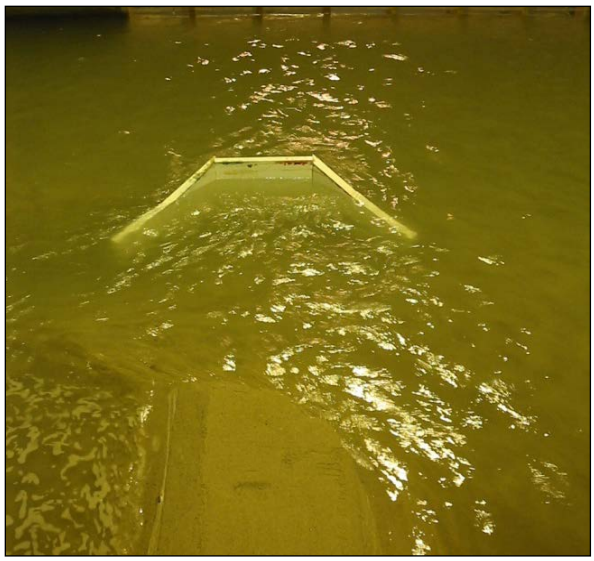

Figure 1. Breach development in a non-cohesive embankment in a lab model (1:30-scale) of a wingwall abutment (Ettema et al. 2010). Bridge abutments typically are wingwall or spill-through forms. Bridge abutments that end with vertical walls and side wings are called "wingwall abutments"; bridge abutnents that end in spill-slopes (where the sideslope form extends around the abutment, are called "spill-through abutments." Most of the experiments in this paper involved spill-through abutments.

2. LABORATORY EXPERIMENTS

2.1. Flume Experiments

Our experiments used a 1:30 geometric-scale, hydraulic model of simulated earthen embankments for spill-through abutments configured as shown in Figure 2. The embankment's top width of 0.40m simulated a standard road having two, 4m wide lanes and 2.4m wide shoulders. The experiments were run using a 18.3m long by 2.4m wide flume, which comprised a sediment recess located in the flume floor between upstream and downstream immovable channel beds. Figure 2 shows the recess and embankment. Recirculation of water for continuous flow through the flume was controlled by a variable frequency-drive pump that, for all the experiments, discharged at $0.11 m^3/s$; producing an average approach-flow velocity of 0.30m/s and flow depth of 0.15m upstream of the model abutment. Fuller (2010) and Chakradhar (2014) document the details of the experiments.

We built simulated earthen embankments for model spill-through abutments placed on a 0.3m-thick sediment recess filled with compacted uniform medium sand as shown in Figure 2. Sand bed was compacted uniformly prior the construction of each abutment model. Penetration resistance tests using a needle penetrometer performed along the transverse line of abutment helped ensure consistent compaction of the sand bed. At least three measurements were recorded on the compacted sand bed at intervals of 0.30m from the toe of abutment spill-slope to the flume's plywood wall as shown in Figure 4a. The 0.2m-thick abutment model consisted of a 1:1.5 erodible spill-through face and side slope formed using soil materials with different shear strengths, including a non-erodible abutment formed of sheet metal and resting on the erodible sand bed.

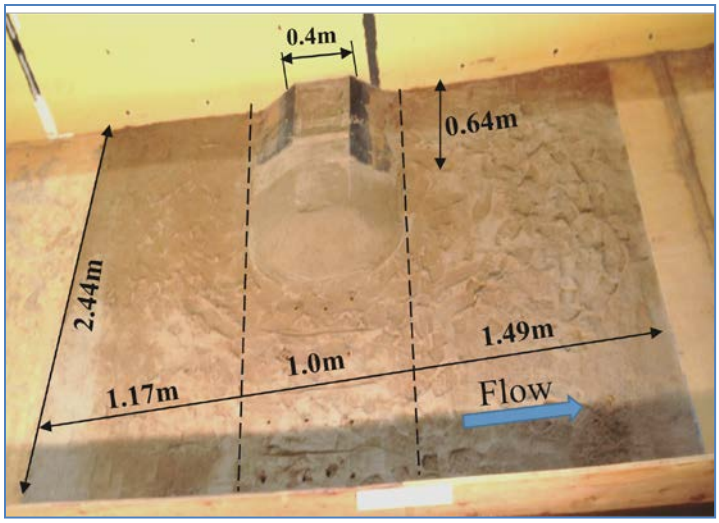

Figure 2. The 1:30-scale earthen embankment for a spill-through abutment located on the sediment recess in a pre-run condition

2.2 Preparation of Model Embankments

Three model soils were used to model earthen embankments: a non-cohesive model soil; a weakly cohesive model soil; and a mixture of these two soils. These soils required different methods for determining their shear strengths. Figures 3 and 4 illustrate embankment preparation and testing. Given the difficulties in flume experiments involving soil strength, we have elaborated on the background soil testing conducted to determine the shear-strength properties of the model soils. Our soil-strength tests followed standard testing practice, and are described here so as to assist other researchers contemplating experiments entailing combined hydraulic and geotechnical processes; see Ng et al. (2015) or Chakradhar (2014) for details on the specific ASTM references.

Construction procedures for the embankment formed of weakly cohesive model soil, which consisted of a clayey-sand, involved careful compaction of the model soil. The target densities were achieved by mixing the clayey sand with calculated moisture content and compaction effort (Figure 3a). Spreading of soil, sprinkling water and mixing were carried out carefully to produce a homogeneous soil. The soil was compacted in layers in the test section. Figures 3b and 4b show the locations of 15 torsional vane shear tests performed on a clayey sand abutment to ensure compaction consistency. The in-situ shear strength of the compacted clayey sand was determined based on a correlation relationship developed for using the torsional vane shear tester (Figure 3b).

The series of experiments involving embankments formed of a non-cohesive model soil (uniform medium sand) whose shear strength was varied by means of different extents of compaction. Water added to sand to produced an approximate 10% moisture content necessary to facilitate compaction. The model sand was spread and compacted in successive layers using a 203mm by 203mm, 4.65kg flat tamper. When the layer thickness reached 100mm, the sand was compacted around the slope edges so as to maintain a slope of 1 vertical to 1.5 horizontal. While compacting close to the edge of a layer, a support to the slope surface was provided using a rectangular flat plate trowel to prevent collapse due to lateral pressure and vibration. This support helped to maintain a smooth side-slope. Penetration resistance measurements using a needle penetrometer and moisture content were recorded before each flume experiment. At least five in-situ penetration resistance tests were performed on soil at the top of the embankment as shown in Figure 3c to ensure compaction consistency. To hydrate the soil model, the embankment model was left for a day before the flume experiment was performed.

It was difficult to quantify the shear strength of different model soils used in the flume experiments. Because forces at model scale reduce in accordance with the length scale cubed (e.g., ASCE 2000), values of strength and stresses for the model soil vary with the length scale of the model; i.e., the force scale divided by the area scale = $L^3/L^2 = L$, the length scale. Therefore, the present study required shear strengths about $1/L = 1/30^{th}$ of shear strengths at actual

abutments. Field values of soil strength in earthen embankments depend on several factors, most notably embankment height. They usually would be in the range of about 50 to 500kPa.

(a) (b) (c)

Figure 3. Preparation of model embankments for spill-through abutments: (a) compaction; (b) torsional-vane test of cohesive soil; and (c) needle penetrometer test

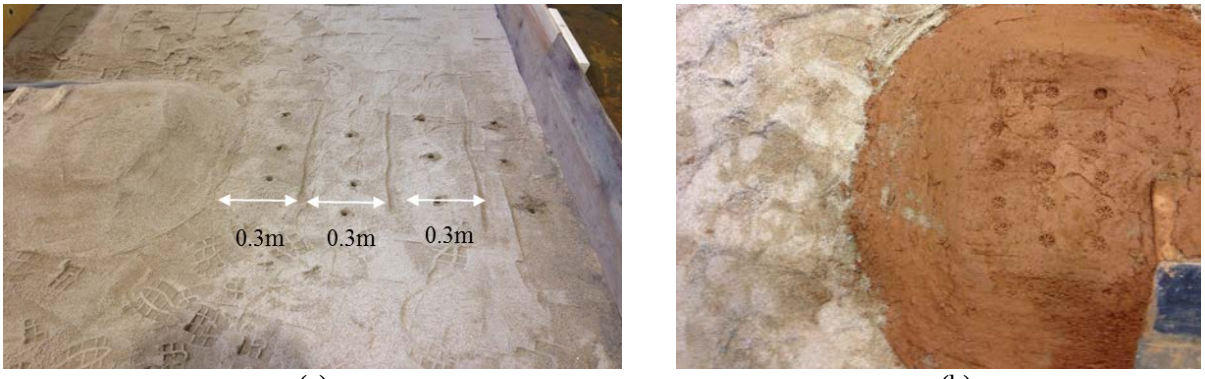

(a) (b)

Figure 4. Test patterns: (a) penetration resistance tests on the sand bed at 0.3m intervals; and, (b) fifteen torsional vane shear tests of the cohesive soil embankment

A further difficulty was that the relatively small size and modest thickness of the model abutments complicated accurate measurement of soil strength. Furthermore, a standard soil-testing device was not available to monitor and closely control the strength of model soil used to form the small size model spill-slope abutment. In fact, actual in-situ soil testing equipment is intended for, and works best with, thick soil formations. We addressed this difficulty by developing an indirect approach to determine shear strengths of uniform sand and clayey sand. Our approach customized in-situ test devices commonly used for strength testing soils. We performed a series of laboratory soil experiments to calibrate the measurements obtained from in-situ test devices with exact strengths obtained with the model soils whose strength properties were adjusted in the controlled circumstances of a geomechanics laboratory. Correlation charts developed based on the proposed calibration procedures were used for quantifying the shear strengths of model spill-through abutments constructed in the flume experiments. Calibration procedures were proposed for both non-cohesive and cohesive model soils as described in the following sections.

2.2.1 Shear Strength of Non-cohesive Soil

The particle size distribution of the non-cohesive model soil, the uniform sand, was performed in accordance with the standard practice specified by the American Society for Testing and Materials, ASTM D422, and was classified as a poorly graded (uniform) sand (SP) as per the USCS, ASTM D2487. Relative density (D_r) tests to determine maximum and minimum dry index unit weights of sand were carried out in accordance with other testing standards, ASTM

D4253 and ASTM D4254, respectively. The maximum dry index unit weight was determined to be 17kN/m^3, with a minimum void ratio of 0.53. The minimum dry index unit weight was 13.9kN/m^3 at a maximum void ratio of 0.87. Seven sand samples were prepared using mould containers to attain relative densities ranging from 50 to 100%. Because actual sand abutments are generally compacted with D_r values well above 50%, which is an index property and not scale dependent, testing on sand samples with D_r values less than 50% was not needed. To achieve a series of relative densities, several methods were used, ranging from manual tapping on the mould using a steel rod, to changing the total surcharge load during vibration with a shake-table.

A needle penetrometer, consisting of a spring-loaded plunger with a needle attached to its end was used to determine the penetration resistance (R) of each compacted sand sample. Although the needle penetrometer was developed for testing fine grained soils, a similar test procedure was adopted here as an approach for controlling sand compaction in the flume experiments. The test procedure of pushing a needle into sand is analogous to pushing an electric cone penetrometer during a cone-penetration test or a split-spoon sampler during a Standard Penetration Test. Using this analogy, it is justifiable to adopt the needle penetrometer test on sand in this study. A minimum of three penetration tests using the needle penetrometer were carried out on each compacted sand sample. We obtained an excellent correlation with a coefficient of determination (r^2) of 0.95 between penetration resistances (R) and relative densities. This correlation further validates the application of the needle penetrometer on sand. It also shows that greater compaction has a greater penetration resistance. Note that test data were not available between 82 and 100%, because compaction within this range could not be controlled reliably, despite of many attempts. We attribute this difficulty to the smaller range of unit weights; from 16.4kN/m^3 to 17kN/m^3 in a relatively higher range of relative densities from 82 to 100%.

A series of direct shear tests, performed in accordance with ASTM D3080, on sand samples compacted to three targeted relative densities of 50%, 60% and 80%. The tests were performed at relatively low effective normal stresses, σ', ranging from 15 to 125kPa. Nonlinear failure envelopes were observed, because the compaction caused interlocking and dilation of sand particles during shearing. Sand samples compacted in thicker layers could not produce a consistent D_r of 50%. We ascribe this difficulty to the greater effect of compacting forces on the top layer compared to underlying layers. In order to generate a reliable failure envelope, seven direct shear tests were carried out on this sand. In contrast, the compaction of thin sand layers for D_r of 60 and 80% produced more consistent results. Thus, only four direct tests were performed on sands for D_r of 60 and 80%. Using the failure envelopes developed for the sand, and the effective normal stresses calculated based on a 200-mm thick model sand abutment with a water level at 140 mm, shear strengths, τ, were related to the corresponding relative densities. The correlations developed were then used to quantify the shear strength of the sand compacted in the flume experiments. The non-cohesive soil shear strength of an actual scale abutment (τ_{actual}) can be related to the shear strength of the model soil (τ_{model}) using Equation (1):

$$\tau_{actual} = \left[\sum\left(\gamma \times d_{model}\right) - u_w\right](SF)\tan\phi = \left(\sigma'_{model}\tan\phi\right)\times SF \quad (1)$$

Here, γ is the soil unit weight, d_{model} is the model soil depth, SF is the scale factor (i.e., 30 used in this experiment), u_w is the hydrostatic pore water pressure (i.e., $\gamma_w \times d_w$), γ_w is the unit weight of water, d_w is the water depth, ϕ is the soil friction angle, and σ'_{model} is the effective normal stress of the model soil. Ng et al. (2015) gives the strength relations developed for the sand.

2.2.1 Shear Strength of Cohesive Soil

Similar to the tests with the non-cohesive model soil (sand), a series of standard laboratory soil tests were performed to classify and determine basic properties of the cohesive model soil (clayey sand). Ng et al. (2015) and Chakradhar (2014) give details regarding these tests, which were –

1. Particle size distribution and hydrometer tests (ASTM 422);
2. Atterberg limit tests (ASTM 418); and,
3. Standard Proctor compaction tests (ASTM 698).

This model soil was classified as clayey sand (SC), per USCS (ASTM 422). The liquid limit and plastic limit were determined as 23 and 16, respectively. It is certain that this clayey soil does not contain sensitive clay minerals, such as Montmorillonite and Illite. Its maximum dry unit weight, $\gamma_{d\text{-}max}$, was determined to be 19.45 kN/m^3 and the corresponding optimum moisture content, ω_{opt}, was 12%. After completing a standard Proctor test, we used a laboratory miniature vane shear device, in accordance with ASTM D4648, to determine the undrained shear strength, S_u, of the compacted clayey sand. We performed a minimum of four vane shear tests on each soil sample. These tests were repeated on soil samples compacted from 89% to 100% of $\gamma_{d\text{-}max}$. Similar compaction was not feasibly performed on soil samples at the wet-side of ω_{opt} at dry unit weights less than 89% of $\gamma_{d\text{-}max}$ (i.e., at a higher moisture content), because adhesion of soil to the Proctor hammer hindered the compaction process. Also, tests were not performed on clayey sand at the dry-side of ω_{opt}, because it was difficult to obtain an adequate penetration and rotation of the vane shear tester on the soil. We found it best if the clayey sand model abutments were compacted at the wet-side of ω_{opt}. Based on these test results, we developed a relationship between percent compaction and S_u.

A series of direct shear tests determined the cohesion and friction angle of the clayey sand in accordance with ASTM D3080. To control the dry unit weight of clayey sand samples for the direct shear test, we used the following soil-sample preparation steps:

1. Clayey sand was compacted in a standard 101.6mm-dia. mould in accordance with ASTM D698;
2. Using a soil extruder, the compacted soil was pushed from the mold into a 63.5mm diameter thin-wall Shelby tube with a metal plate custom-made to collect a 63.5mm diameter undisturbed soil sample. The process of sampling the soil into the Shelby tube was carried out with caution to minimize soil disturbance and prevent any loss of moisture;
3. Soil collected in the Shelby tube was extruded and trimmed into a 25.4mm length without crumbing the soil;
4. During the trimming process, a smooth cut surface was required to ensure a uniform distribution of the normal stress applied during the direct shear test; then,
5. The prepared soil sample was placed into the 63.5mm diameter shear box for a subsequent direct shear test.

Direct shear tests done on clayey sand samples prepared at 91, 97 and 98% of $\gamma_{d\text{-}max}$, to determine the respective failure envelopes for the soils. The cohesion values and friction angles determined from the direct shear tests were used to ascertain the corresponding normal stress at the model abutment depth of 200 mm, τ, using the linear Mohr-Coulomb failure relationship and related to percent compaction. This relationship showed that shear strength of clayey sand increased with increasing percent compaction. The percent compaction of clayey-sand model abutments constructed for the flume experiments was estimated based on the S_u value measured using the vane shear tester. Knowing the percent compaction, we could use the correlation to estimate the shear strength of the model soil forming model abutment. Similar to Eq. 1 for the non-cohesive soil, cohesive soil shear strength of an actual scale abutment (τ_{actual}) can be related to the shear strength of the model soil (τ_{model}) using Eq. (2):

$$\tau_{actual} = \left[\sum\left(\gamma \times d_{model}\right) - u_w\right](SF)\tan\phi + c = \left(\sigma'_{model}\tan\phi\right)(SF) + c \qquad (2)$$

where, γ is the soil unit weight, d_{model} is the model soil depth, SF is the scale factor (i.e., 30 used in this experiment), u_w is the hydrostatic pore water pressure (i.e., $\gamma_w \times d_w$), γ_w is the unit weight of water, d_w is the water depth, ϕ is the soil friction angle, c is the soil cohesion, and σ'_{model} is the effective normal stress of the model soil.

3. RESULTS

3.1 Strength Properties of Model Embankments

We achieved reasonable success in controlling the overall strength properties of model earthen embankments in laboratory flume experiments, and quantifying the shear strength of such embankments. However, we also encountered some difficulties. The ensuing points briefly discuss our main findings.

While consistent compaction of the model soil was achieved by building the model abutments in successive layers, and controlling the amount of compaction effort and moisture content, additional care was given when applying the

same compaction procedure on and near the abutment's spill-slope, where soil thickness thinned to zero. Careful attention had to be given to forming the model embankments and preventing their collapse due to compaction.

We saw that errors may accumulate in the correlation methods for soil shear strength estimation. These errors could affect the accuracy of the estimated soil shear strength, which is an important factor in the scour investigation. Fortunately, the sound correlations obtained from this study (i.e., correlation coefficient greater than 0.8) will minimize these errors. A direct measurement of soil shear strength in flume experiments will be a good option if an in-situ measurement device, such as a miniature electric cone penetrometer and soil/water pressure meter, is available. This device will improve the efficiency of performing flume experiments and increase the accuracy of shear strength measurements. In-situ shear strength was quantified on the flat surface of model soil abutments, as illustrated in Figures 5 and 6, using the correlations developed based on hand-held devices. Since the scour process is influenced by the combination of geotechnical and hydraulic processes on the compacted spill-slope surface, it is reasonable to determine the shear strength of soil on or near the slope.

Changes in the shear strength of model soils before and after filling the flume with water as well as during an experiment were very difficult to quantify. With the flume filled with water, the development of negative capillary pressure in model soils above the water level due to initial wetting created an apparent cohesion, which attracted soil particles and contributed additional shear strength. However, the continuous wetting of model soils over time and during flume experiments could destroy this apparent cohesion. These changes in soil shear strength explain the typical abutment failure mode observed in the flume experiment: under-cutting at abutment toe, development of tension cracks at abutment crest and subsequent toppling of soil blocks.

Consistent compaction of the simulated sand bed floodplain was required between each experiment in order to make them comparable. Although uniform and consistent compaction as well as the tests to confirm the consistency was a big challenge, the procedure developed based on the needle penetrometer provided an adequate control.

A scale effect that aided the present experiments using sand as model soil was the capillary action of water in sand. Surface tension within water, and adhesion of water to sand, elevated the water surface within the dry sand about 55mm above the elevation of stationary water in the flume, coinciding with the estimated meniscus rise for water in a medium having 0.70mm diameter openings (Batchelor 1967). Capillary rise contributed apparent cohesion to the behaviour of sand in the zone of capillary rise (practically the full height of model abutment above the waterline), and thereby enabled wet sand exposed to air to stand with a vertical face and fail in blocks. The shear strength of sand in the capillary zone is –

$$\tau = \sigma'_v \tan(\phi) = \left[\gamma z + \gamma_w (D - z)\right]\tan(\phi) = (\gamma - \gamma_w) z \tan(\phi) + D\gamma_w \tan(\phi) \quad (3)$$

where D is the depth of the capillary zone (i.e., 55mm); z is the depth below the abutment's top; and ϕ is the friction angle of the sand. Apparent cohesion altered the as-built strength of the model abutments formed of sand, and caused the model abutment to behave as if it had a layer of weakly cohesive soil immediately above the waterline. The writers found that the model abutments formed of compacted sand and sand-clay mix could therefore visually replicate the main failure processes associated with riverbank erosion. The clayey sand was much less permeable and did not exhibit the same extent of capillary rise during the relatively short duration of an experiment.

3.2 Flume Experiments on Bridge-Embankment Erosion

Our scour experiments led to bridge embankment erosion in a manner analogous to erosion widening of an embankment breach. As scour developed it began to undercut the embankment spillslope immediately adjacent to the scour depression forming in the sand bed. Scour also began along the sandy floodplain at a location slightly downstream of the abutment's centerline. It is well-known that flow field contraction and turbulence cause scour to begin at these locations. However, immediately noticeable along the waterline at the upstream corner of each model abutment were swift flow velocities and energetic water-surface oscillation and turbulence associated with flow contraction and separation at the abutment's upstream corner; as Figures 5a&b show. Photographs of dam and levee breaching show that these flow features also develop with breach formation.

The unprotected spillslope began visibly eroding at its upstream corner (Figures 5a&b), as flow hydraulically eroded model soil and undercutting the spillslope at the waterline. What subsequently unfolded was the progressive toppling of blocks of spillslope soil, such that the corner eroded back to form a vertical face along the front of the spill-slope (Figure 5b). A recurring feature of embankment failure was the appearance of tension cracking above each under-cut block of abutment soil, and the action of gravity, eventually caused soil blocks to rotate about a point at the water surface where undermining was greatest. Blocks toppling into the channel were quickly eroded by flowing water, and exposed additional spillslope soil to under-cutting. The observed erosion cycle was essentially the same as often described for eroding riverbanks. No circular, slip-surface failure surface was observed for the spillslopes.

The cycle of under-cutting, toppling, and spillslope erosion continued until the exposed face of the spillslope retreated to form a circular arc at the waterline (Figure 5b); similar to Figure 12 in Brunner (2014). Arc radius, r, approximately fitted the geometry recommended for rounded orifices and nozzles; e.g., for bellmouth nozzles, Brater and King (1976) give $r = 1.63D$, where D = nozzle diameter (or, in the present case, D = waterway surface width across the downstream transect of the bridge). As the spillslope eroded, D increased and the arc flattened in curvature. Figures 6a-c show the erosion forms developed with the non-cohesive, weakly cohesive and cohesive soils.

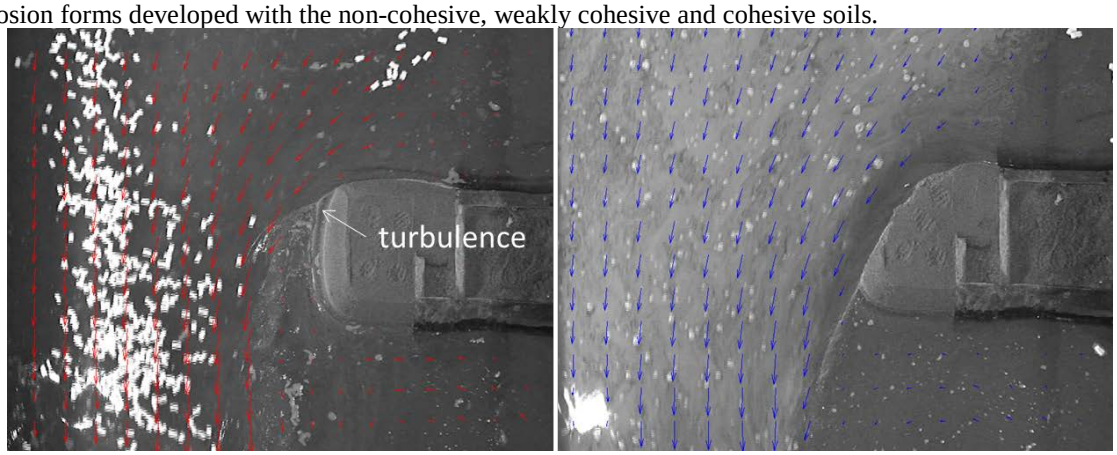

Figure 5. Flow field and evolution of breach plan form.

(a) (b) (c)

Figure 6. Breach formation at a model spill-through abutment: (a) non-cohesive model soil (sand); (b) 80% sand - 20% clay mixture; and, (c) cohesive model soil (water discoloured with eroded clay)

The model spillslopes formed of sand-clay mixtures failed in much the same did the spillslopes of uniform sand, except for two additional factors that complicated the experiments. For the 80% sand - 20% clay mix, flow around the abutment bled clay particles from the failure zone at the spillslope face, reducing model soil strength to essentially that of sand alone. The greater shear strength of the clayey sand model soil resulted in commensurately wider blocks of failed spill-slope soil, and the toppled blocks did not further erode as rapidly as did the sand blocks; consequently, the flow area at the abutment did not increase as rapidly as for the failed weaker abutments formed of sand. Figures 7a&b illustrate how hydraulic erosion undercut the face of the embankment, caused a tension crack to form, and eventually the block detached from the face.

(a) (b)

Figure 7. Erosion of a non-cohesive (sand) embankment: (a) the formation of a tension crack; and (b) eventual detachment of a block from the face of the embankment (dimensions in meters). Note that surface tension gives sand a modicum of cohesion for this small-scale experiment.

The effective soil strengths mentioned herein are the values associated with the model embankments surrounded by water immediately prior to beginning an experiment. Abutment erodibility and soil strength influenced scour depth at the model abutments, although the strength of the model soil was difficult to control and measure immediately at the start of a test. Capillarity effects, along with the bleeding of clay particles from sand-clay mixtures, and the different time rates of scour development on the channel bed and geotechnical erosion of the model spillslope soil complicated interpretation of the influence of soil strength.

Although our paper focuses on the practical considerations of conducting experiments involving combined hydraulic and geotechnical processes involved in breach development, it is useful to mention the overall trend we obtained regarding the influence of model soil strength on scour depth at the end of the model embankment. This information is perhaps pertinent to scour development at a levee that breaches and erodes to its base as the breach widens. Figure 8 presents the maximum scour depths versus the effective shear strength of model abutment formed of the model soil. This figure shows that scour depths obtained with the non-cohesive (sand) embankments were about 25 to 40% of the depth obtained with the non-erodible abutment. The non-erodible abutment was simulated using a metal form placed neatly over the abutment structure. The non-erodible abutment has the same dimensions shown in Figure 2. For the lower values of shear strength, the measured maximum scour depths were practically constant for the uniform sand, owing to the difficulty of controlling the compaction of sand forming the spill-slope. Only for the most densely compacted and stronger model embankments was the soil strength in the spill-slope appreciably greater than that for the weaker model embankments. The scour depths obtained with abutments formed of the weakly cohesive model soil approached 65 to about 80% of the depth obtained with the erosion resistant abutment, and these depths were larger than obtained with the abutments formed of the non-cohesive model soil.

The scour depths measured near the model abutments formed of non-cohesive model soil (sand) compacted to a range of densities were found to correlate with soil shear strength, although only when soil strength exceeded a value of about 8.0kPa. For soil strengths less than this value, scour depths varied little with soil strength. This trend occurred largely because the strength of the spill-slope soil was difficult to control consistently for the less compacted sands. For soil (sand) strengths above about 8.0kPa, scour depth increased with increasing soil (sand) strength.

The experiments showed that abutments constructed with higher compacted soils, which exhibit higher shear strengths, required a longer time of abutment erosion before achieving an equilibrium state in the failure process (Chakradhar 2014). Thus, a slower erosion rate of a higher strength spill-slope provides a longer time and higher flow velocity to erode the sand bed (i.e., river bed), causing a deeper scour. These experimental results clearly illustrate the interactive geotechnical and hydraulic processes in influencing the scour depth and abutment erosion.

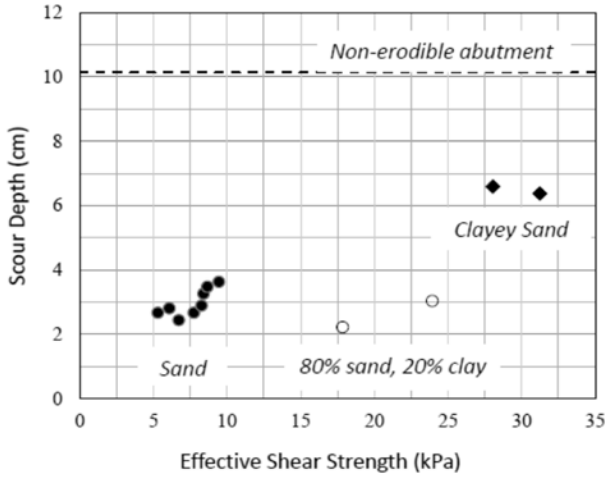

Figure 8. Flume data on maximum scour depth versus effective shear strength of model soil.

4. CONCLUDING COMMENT

Our paper offers insights regarding the widening of breaches formed in earthen embankments. The insights were obtained from experiments on scour at erodible bridge-waterway abutments. Contemporary investigation of bridge-abutment scour is grappling with how to simulate the combined effects of the geotechnical and hydraulic processes associated with scour. Further research on breach development in earthen embankments must also grapple with this same issue.

5. REFERENCES

ASCE (2000). Hydraulic Modeling: Concepts and Practice. ASCE Publications, Reston VA.

ASCE Task Committee on Dam/Levee Breaking (2011), "Earthen embankment breaching." Journal of Hydraulic Engineering, ASCE, 137(12), 1549-1562.

Batchelor, G. K. (1967), An Introduction to Fluid Dynamics, Cambridge University, Cambridge UK, 67.

Brater, E. F. and King, H. W. (1976). Handbook of Hydraulics. McGraw-Hill Inc., New York, NY, 4-20.

Brunner, G. (2014), Using HEC-RAS for Dam Break Studies. Report TD-39, US Army Corps of Engineers, Davis, CA.

Chakradhar R.S. (2014), Laboratory Investigation of Geotechnical and Hydraulic Influences on Abutment Scour. MS Thesis, University of Wyoming, Laramie WY.

Ettema R, Nakato T. and Muste M. (2010), Estimation of Scour Depth at Bridge Abutments. Washington, D.C. (USA): National Cooperate Highway Research Program, NCHRP 24-20, Transportation Research Board.

Ettema, R., Ng, K.W., Chakradhar, Fuller, J. and Kempema, E. (2015), Failure of spill-through bridge abutments during scour: flume and field observations." Journal of Hydraulic Engineering, ASCE, 142(5), DOI: 06015001.

Feliciano-Cestero J.A., Imran J., and Chaudhry M.H. (2014), Experimental investigation of the effects of soil properties on levee breach by overtopping. Journal of Hydraulic Engineering, ASCE, 04014085, 1-14.

Fuller J. (2010), Geotechnical and Hydraulic Processes during Scour at Spill-through Bridge Abutments. MS Thesis, University of Wyoming, Laramie, WY.

Morris M., Hassan M., and Vaskinn, K. (2007), "Breach formation: field test and laboratory experiments." Journal of Hydraulic Research, 45(1), 9-17.

Ng. K.W., Chakradhar, R. Ettema, R. and Kempema, E. (2015), "Geotechnical considerations in hydraulic modeling of bridge abutment scour. Journal of Applied Water Engineering and Research, 3(2), 132-142.